



Available online at www.sciencedirect.com

ScienceDirect

Comput. Methods Appl. Mech. Engrg. 395 (2022) 115031

Computer methods in applied mechanics and engineering

www.elsevier.com/locate/cma

High-order space–time finite element methods for the Poisson–Nernst–Planck equations: Positivity and unconditional energy stability[★]

Guosheng Fu*, Zhiliang Xu

Department of Applied and Computational Mathematics and Statistics, University of Notre Dame, USA

Received 3 May 2021; received in revised form 25 March 2022; accepted 15 April 2022

Available online 12 May 2022

Abstract

We present a novel class of high-order space-time finite element schemes for the Poisson-Nernst-Planck (PNP) equations. We prove that our schemes are mass conservative, positivity preserving, and unconditionally energy stable for any order of approximation. To the best of our knowledge, this is the first class of (arbitrarily) high-order accurate schemes for the PNP equations that simultaneously achieve all these three properties.

This is accomplished via (1) using finite elements to directly approximate the so-called *entropy variable* $u_i := U'(c_i) = \log(c_i)$ instead of the density variable c_i , where $U(c_i) = (\log(c_i) - 1)c_i$ is the corresponding entropy, and (2) using a discontinuous Galerkin (DG) discretization in time. The *entropy variable* formulation, which was originally developed by Metti et al. (2016) under the name of a *log-density formulation*, guarantees both positivity of densities $c_i = \exp(u_i) > 0$ and a continuous-in-time energy stability result. The DG in time discretization further ensures an unconditional energy stability in the fully discrete level for any approximation order, where the lowest order case is exactly the backward Euler discretization and in this case we recover the method of Metti et al. (2016). © 2022 Elsevier B.V. All rights reserved.

MSC: 65N30; 65N12; 76S05; 76D07

Keywords: Poisson-Nernst-Planck equation; Energy stability; Positivity preservation; Entropy variable; Space-time FEM

1. Introduction

The Poisson–Nernst–Planck (PNP) equations describe the diffusion of charged particles under the effect of an electric field that is itself affected by these particles. This system of equations has been widely used in the modelling of semiconductors [1] and ion channels in biology [2].

Various numerical methods with different properties have been developed for the PNP equations [3–8]. We particularly cite the very recent schemes [9–14] that were provably positivity preserving for the particle densities and

E-mail addresses: gfu@nd.edu (G. Fu), zhiliangxu@nd.edu (Z. Xu).

[☆] G. Fu acknowledges the partial support of this work from U.S. National Science Foundation through grant DMS-2012031. Z. Xu was partially supported by the U.S. National Science Foundation CDS&E-MSS 1854779.

^{*} Corresponding author.

unconditionally energy dissipative for the free energy, among which the schemes in [9-13] are first-order accurate in time, while the scheme in [14] is high-order accurate in time but the associated energy dissipation law is only valid for a modified energy due to the use of the recent scalar auxiliary variable (SAV) technique [15]. To the best of our knowledge, no provable positivity preserving and unconditionally energy dissipative scheme for the original energy that is at least second-order accurate in time exists so far. We fill this gap by presenting a class of arbitrarily high-order accurate space-time finite element (STFEM) schemes satisfying these properties. The major novelty of our approach is the seamless combination of a finite element spatial discretization using the entropy variables and a novel discontinuous Galerkin (DG) temporal discretization for the resulting differential-algebraic (DAE) system. Our spatial discretization is the finite element scheme proposed by Metti et al. [9] that is based on a log-density formulation, which is similar in spirit to the entropy-stable schemes based on the so-called entropy variables for hyperbolic conservation laws and compressible flow in the CFD literatures [16–19]. The use of finite elements to approximate the entropy variable $u_i = \log(c_i)$ instead of the density variable c_i mainly serves two purposes: (1) density $c_i := \exp(u_i)$ is guaranteed to be positive, and (2) semi-discrete energy-stability is achieved using classical energy variational arguments. Due to the highly nonlinear nature of the resulting DAE system, it is difficult to design a proper time stepping strategy that yields a high-order fully-discrete energy stable scheme. As a matter of fact, only the first-order backward Euler scheme was shown to be energy stable [9]. In particular, fully-discrete energy stability cannot be proven for the standard high-order finite-difference based time stepping strategies like the second-order Crank-Nicolson method, the high-order BDF methods, or the diagonally implicit Runge-Kutta methods. The key contribution of this work is the use of a variational finite-element based high-order time stepping strategy for this DAE system, which guarantees unconditional energy stability. To achieve this, we use an upwinding DG time integrator for the density equations combined with a novel Gauss-Radau projection based DG integrator for the (algebraic) electrostatic potential equation. Thanks to the unconditional energy stability result, we can adaptively select the time step size mainly by accuracy conditions. Hence we also discuss adaptive time stepping using the classical proportional integral (PI) step size controller [20].

Since the PNP equations can be viewed as a Wasserstein gradient flow [21], we expect our STFEM scheme with *entropy variables* can be applied to construct high-order positivity preserving and unconditionally energy stable schemes for other Wasserstein gradient flow problems, like the Fokker–Planck equation and the porous medium equation.

The rest of the paper is organized as follows. In Section 2, we first introduce the PNP equations then present the spatial/temporal finite element discretizations and prove that they are mass conservative, positivity preserving, and unconditionally energy dissipative. We further discuss about the nonlinear system solver via the Newton's method and adaptive time step size control. Numerical results are presented in Section 3. We conclude in Section 4.

2. The PNP equations and the space-time finite element schemes

2.1. PNP equations

We consider the PNP equations with N species of charged particles [22] on a bounded domain $\Omega \subset \mathbb{R}^d$, d = 1, 2, 3, with boundary $\partial \Omega$:

$$\frac{\partial c_i}{\partial t} = \nabla \cdot (D_i c_i \nabla \mu_i), \quad i = 1, 2, \dots, N,$$
(1a)

$$-\nabla \cdot (\epsilon \nabla \phi) = \rho_0 + \sum_{i=1}^{N} z_i e c_i, \tag{1b}$$

where c_i is the density of the *i*th charged particle species, D_i is the diffusion constant,

$$\mu_i := \log(c_i) + \frac{z_i e}{k_B T} \phi$$

is the chemical potential of the *i*th species, z_i is the valence, e is the unit charge, k_B is the Boltzmann constant, T is the absolute temperature, ϵ is the electric permittivity, ϕ is the electrostatic potential, ρ_0 is the permanent (fixed) charge density of the system, and N is the number of charged particle species.

The PNP system (1a)–(1b) is closed with the following set of initial and boundary conditions:

$$c_i(0, x) = c_i^0(x), \quad \text{in } \Omega$$
 (1c)

$$c_i \frac{\partial \mu_i}{\partial n} = \frac{\partial \phi}{\partial n} = 0, \quad \text{on } \partial \Omega.$$
 (1d)

Here for simplicity, we use the homogeneous Neumann boundary condition for the charged particle densities. Other boundary conditions will be used in our numerical experiments. Note that the electrostatic potential ϕ is determined up to a constant due to the pure Neumann boundary condition. Following the classical convention, we select a unique ϕ by requiring

$$\int_{\Omega} \phi \, \mathrm{d} x = 0.$$

The PNP system (1) satisfies the following three important properties:

(i) Mass conservation:

$$\int_{Q} c_i(t, x) dx = \int_{Q} c_i^0(x) dx.$$
 (2a)

(ii) Positivity preservation:

If
$$c_i^0(x) > 0$$
, then $c_i(t, x) > 0$ for any $t > 0$. (2b)

(iii) Energy dissipation:

$$\frac{d}{dt}E = -\sum_{i=1}^{N} \int_{\Omega} D_i c_i |\nabla \mu_i|^2 dx,$$
(2c)

where $E(\{c_i\}, \phi) := \int_{\Omega} \left(\sum_{i=1}^{N} (c_i(\log(c_i) - 1)) + \frac{1}{2} \frac{\epsilon}{k_B T} |\nabla \phi|^2 \right) dx$ is the total free energy.

Remark 2.1. The above energy dissipation (2c) is obtained by a standard energy variational argument, where, in particular, one multiplies Eq. (1a) with the test function $\mu_i = \log(c_i) + \frac{z_i e}{k_B T} \phi$ and integrates over the domain Ω . An immediate consequence is that such energy dissipation would fail to hold in a standard finite element discretization where one only approximates the fields c_i and ϕ using finite elements.

One approach to recover energy stability is to use a log-density formulation [9], where one directly discretizes the *entropy variables*

$$u_i = U'(c_i) = \log(c_i),\tag{3}$$

instead of the densities c_i , where $U(c_i) := c_i(\log(c_i) - 1)$ is the entropy of the *i*th species. In this formulation, the species densities $c_i(u_i) := \exp(u_i)$ are *derived* variables which are guaranteed to stay positive $c_i = \exp(u_i) > 0$ for any time t > 0. We point out that such *entropy-variable* based schemes are similar in spirit to the entropy stable schemes using *entropy variables* for hyperbolic conservation laws and compressible flow [16–19].

To this end, we work with the following reformulated PNP equations (1a)–(1b):

$$\frac{\partial \exp(u_i)}{\partial t} = \nabla \cdot \left(D_i \exp(u_i) \left(\nabla u_i + \frac{z_i e}{k_B T} \nabla \phi \right) \right), \tag{4a}$$

$$-\nabla \cdot (\epsilon \nabla \phi) = \rho_0 + \sum_{i=1}^{N} z_i e \exp(u_i). \tag{4b}$$

2.2. Spatial discretization

Let $\mathcal{T}_h := \{K\}$ be a conforming simplicial triangulation of the domain Ω . We shall use the following conforming finite element space

$$V_h^k := \{ v \in H^1(\Omega) : \ v|_K \in \mathcal{P}_k(K), \quad \forall K \in \mathcal{T}_h \}, \tag{5}$$

where $\mathcal{P}_k(K)$ is the space of polynomials of degree at most $k \geq 1$ on K.

The spatial discretization of our finite element scheme for Eqs. (4) with initial and boundary conditions (1c)–(1d) reads as follows: Find $u_{h,1}, \ldots, u_{h,N} \in V_h$ and $\phi_h \in V_h$ with $\int_{\Omega} \phi_h dx = 0$ such that, for t > 0,

$$\int_{\Omega} \frac{\partial \exp(u_{h,i})}{\partial t} v_i \, \mathrm{dx} + \int_{\Omega} D_i \exp(u_{h,i}) \left(\nabla u_{h,i} + \frac{z_i e}{k_B T} \nabla \phi_h \right) \cdot \nabla v_i \, \mathrm{dx} = 0, \quad \forall v_i \in V_h,$$
 (6a)

$$\int_{\Omega} \epsilon \nabla \phi_h \cdot \nabla \psi \, d\mathbf{x} - \int_{\Omega} \left(\rho_0 + \sum_{i=1}^{N} z_i e \exp(u_{h,i}) \right) \psi \, d\mathbf{x} = 0, \quad \forall \psi \in V_h, \tag{6b}$$

with initial conditions

$$u_{h,i}(0,x) = \log(c_i^0(x)), \quad i = 1, 2, \dots, N.$$

The following results show that the semi-discrete scheme (6) satisfies the three properties (2).

Theorem 2.1. Assume $c_i^0 > 0$ for all i. Then the three properties (2) are satisfied for the solution to the semi-discrete scheme (6), where the densities c_i in (2) are given explicitly as $c_i = \exp(u_{h,i})$.

Proof. Taking $v_i = 1$ in (6a), we get mass conservation property (2a). Positivity property (2b) following directly by the definition of $c_i = \exp(u_{h,i}) > 0$.

Let us prove the energy dissipation property (2c). Denoting $\mu_{h,i} := u_{h,i} + \frac{z_i e}{k_B T} \phi_h \in V_h$, taking test function $v_i = \mu_{h,i}$ in (6a) and adding, we get

$$\sum_{i=1}^{N} \int_{\Omega} \frac{\partial \exp(u_{h,i})}{\partial t} \mu_{h,i} \, \mathrm{d}\mathbf{x} + \sum_{i=1}^{N} \int_{\Omega} D_{i} \exp(u_{i}) |\nabla \mu_{h,i}|^{2} \, \mathrm{d}\mathbf{x} = 0.$$

A simple calculation yields that

$$\int_{\Omega} \frac{\partial \exp(u_{h,i})}{\partial t} u_{h,i} \, \mathrm{d} x = \frac{d}{dt} \int_{\Omega} \underbrace{\exp(u_{h,i})(u_{h,i} - 1)}_{:=U(u_{h,i})} \, \mathrm{d} x.$$

Hence,

$$\sum_{i=1}^{N} \frac{d}{dt} \int_{\Omega} U(u_{h,i}) dx + \int_{\Omega} \sum_{i=1}^{N} \frac{z_i e}{k_B T} \frac{\partial \exp(u_{h,i})}{\partial t} \phi_h dx + \sum_{i=1}^{N} \int_{\Omega} D_i \exp(u_i) |\nabla \mu_{h,i}|^2 dx = 0.$$
 (7)

Taking $\psi = \frac{\partial \phi}{\partial t}/(k_B T)$ in Eq. (6b) and subtract the resulting expression from (7), we get

$$\frac{d}{dt}E_h + \sum_{i=1}^N \int_{\Omega} D_i \exp(u_i) |\nabla \mu_{h,i}|^2 dx = 0,$$

where the discrete free energy

$$E_h := \int_{\Omega} \left(\sum_{i=1}^N U(u_{h,i}) + \sum_{i=1}^N \frac{z_i e}{k_B T} \exp(u_{h,i}) \phi_h - \frac{\epsilon}{2k_B T} |\nabla \phi_h|^2 + \frac{\rho_0}{k_B T} \phi_h \right) \mathrm{dx}.$$

Taking $\psi = \phi_h/(k_B T)$ in (6b), we get

$$\int_{\Omega} \sum_{i=1}^{N} \frac{z_i e}{k_B T} \exp(u_{h,i}) \phi_h dx = \int_{\Omega} \left(\frac{\epsilon}{k_B T} |\nabla \phi_h|^2 - \frac{\rho_0}{k_B T} \phi_h \right) dx.$$

Combining the above two expressions, we get

$$E_h = \int_{\Omega} \left(\sum_{i=1}^{N} U(u_{h,i}) + \frac{\epsilon}{2k_B T} |\nabla \phi_h|^2 \right) dx.$$

This completes the proof of (2c). \square

2.3. Temporal discretization

In this subsection, we discretize the differential-algebraic system (6) using a discontinuous Galerkin (DG) time integrator of degree $m \ge 0$. The major advantage of using the DG integrator is that we can prove an unconditional energy stability result for the fully discrete scheme for any polynomial degree $m \ge 0$ in time. To the best of our knowledge, this is the first class of arbitrarily high-order accurate numerical schemes for the PNP equations that are provably positive and unconditionally energy stable.

At the *n*th time level t^n , we denote the time step size as Δt^n and the update time interval as $I^n = [t^n, t^{n+1})$. We denote the space-time finite element space on the space-time slab $\Omega \times I^n$ as follows:

$$\mathsf{V}_{h}^{k,m,n} := \{ v \in H^{1}(\Omega \times I^{n}) : \ v|_{K \times I^{n}} \in \mathcal{P}_{k}(K) \otimes \mathcal{P}_{m}(I^{n}), \quad \forall K \in \mathcal{T}_{h} \},$$

$$(8)$$

The fully discrete scheme then reads as follows: for any $n=1,2,\ldots$, find $u_{h,i}^n\in \mathsf{V}_h^{k,m,n}$ and $\phi_h^n\in \mathsf{V}_h^{k,m,n}$ with $\int_{\mathcal{O}}\phi_h^{n,-}\,\mathrm{d}x=0$ such that

$$\int_{I^{n}} \int_{\Omega} \frac{\partial \exp(u_{h,i}^{n})}{\partial t} v_{i} \, dx dt + \int_{\Omega} \left(\exp(u_{h,i}^{n,+}) - \exp(u_{h,i}^{n-1,-}) \right) v_{i}^{n,+} \, dx \\
+ \int_{I^{n}} \int_{\Omega} D_{i} \exp(u_{h,i}^{n}) \left(\nabla u_{h,i}^{n} + \frac{z_{i}e}{k_{B}T} \nabla \phi_{h}^{n} \right) \cdot \nabla v_{i} \, dx dt = 0, \quad \forall v_{i} \in V_{h}^{k,m,n}, \tag{9a}$$

$$\int_{I^n} \int_{\Omega} \epsilon \nabla \phi_h^n \cdot \nabla \psi \, dx dt - \int_{I^n} \int_{\Omega} \left(\rho_0 + \sum_{i=1}^N z_i e \exp(u_{h,i}^n) \right) \psi \, dx dt = 0, \quad \forall \psi \in \mathsf{V}_h^{k,m-1,n}, \tag{9b}$$

$$\int_{\Omega} \epsilon \nabla \phi_h^{n,-} \cdot \nabla \psi^{n,-} \, \mathrm{d}\mathbf{x} - \int_{\Omega} \left(\rho_0 + \sum_{i=1}^N z_i e \exp(u_{h,i}^{n,-}) \right) \psi^{n,-} \, \mathrm{d}\mathbf{x} = 0, \quad \forall \psi \in V_h^k, \tag{9c}$$

where we denote $\xi^{n,-} := \lim_{t \nearrow t^{n+1}} \xi^n(t,x)$ and $\xi^{n,+} := \lim_{t \searrow t^n} \xi^n(t,x)$.

Remark 2.2. We note that the classical upwinding DG time integrator is used in (9a), and a non-standard Gauss–Radau type projection is used in (9b)–(9c) for the temporal discretization of the Poisson equation. Recall that the Gauss–Radau projection of order m with right endpoint for a function f on the interval I^n is given as follows: find $f_h \in \mathcal{P}_m(I^n)$ such that

$$\int_{I^n} f_h \phi_h \, \mathrm{dt} = \int_{I^n} f \phi_h \, \mathrm{dt}, \quad \forall \phi_h \in \mathcal{P}_{m-1}(I^n),$$

$$f_h(t^{n+1}) = f(t^{n+1}).$$

This Gauss–Radau type projection is necessary for us to prove the unconditional energy stability of the scheme (9) in Theorem 2.2. In particular, for the energy stability proof, we need to take test function $\phi = \partial_t \phi_h^n/(k_B T) \in V_h^{k,m-1,n}$ in (9b) and $\psi = \phi_h^{n,-}/(k_B T) \in V_h^k$ in (9c). We further note that when m = 0, the temporal discretization is simply the following backward Euler method considered in [9]: find $u_{h,i}^n \in V_h^k$ and $\phi_h^n \in V_h^k$ with $\int_{\Omega} \phi_h^n \, dx = 0$ such that

$$\int_{\Omega} \left(\exp(u_{h,i}^{n}) - \exp(u_{h,i}^{n-1}) \right) v_{i} \, dx + \Delta t^{n} \int_{\Omega} D_{i} \exp(u_{h,i}^{n}) \left(\nabla u_{h,i}^{n} + \frac{z_{i}e}{k_{B}T} \nabla \phi_{h}^{n} \right) \cdot \nabla v_{i} \, dx = 0,$$

$$\int_{\Omega} \epsilon \nabla \phi_{h}^{n} \cdot \nabla \psi \, dx - \int_{\Omega} \left(\rho_{0} + \sum_{i=1}^{N} z_{i}e \exp(u_{h,i}^{n}) \right) \psi \, dx = 0,$$

for all $v_i \in V_h^k$ and $\psi \in V_h^k$, where we identified the space-time space $V_h^{k,0,n}$ with the spatial space V_h^k , and used the fact that $\frac{\partial \exp(u_{h,i}^n)}{\partial t} = 0$ and $u_{h,i}^{n,+} = u_{h,i}^{n,-} = u_{h,i}^n$ for $u_{h,i}^n \in V_h^{k,0,n}$, and the integrand in the last term of (9a) is independent of time.

The following results show that the fully-discrete scheme (9) satisfies a discrete version of three properties (2).

Theorem 2.2. Assume $c_i^0 > 0$ for all i. For any solution to the scheme (9), the following three properties holds

$$\int_{\Omega} \exp(u_{h,i}^{n,-}) \, \mathrm{d}x = \int_{\Omega} \exp(u_{h,i}^{n-1,-}) \, \mathrm{d}x,\tag{10a}$$

$$c_{h,i}^{n} := \exp(u_{h,i}^{n}) > 0,$$
 (10b)

$$E_h^n - E_h^{n-1} = -\operatorname{Diss}_h^n - N_{h,1}^n - N_{h,2}^n \tag{10c}$$

where the discrete energy is given by

$$E_h^n := \int_{\Omega} \left(\sum_{i=1}^N U(u_{h,i}^{n,-}) + \frac{\epsilon}{2k_B T} |\nabla \phi_h^{n,-}|^2 \right) d\mathbf{x}, \tag{10d}$$

the (non-negative) physical dissipation term

$$\mathsf{Diss}_h^n := \int_{I^n} \int_{\Omega} \sum_{i=1}^N D_i c_{h,i}^n |\nabla \mu_{h,i}^n|^2 \, \mathrm{d}x \mathrm{d}t,$$

and the (non-negative) numerical dissipation terms $N_{h,1}^n$ and $N_{h,2}^n$ for the temporal discretization are given as follows

$$N_{1,h}^{n} := \int_{\Omega} \sum_{i=1}^{N} \frac{1}{2} \exp(\xi_{h,i}^{n}) (u_{h,i}^{n-1,-} - u_{h,i}^{n,+})^{2} dx,$$

$$N_{2,h}^{n} := \int_{\Omega} \frac{\epsilon}{2k_{B}T} |\nabla(\phi_{h}^{n,+} - \phi_{h}^{n-1,-})|^{2} dx,$$

where $\xi_{h,i}^n$ is a function between $u_{h,i}^{n,+}$ and $u_{h,i}^{n-1,-}$ for each i.

Proof. Again, we only need to prove the energy stability result (10c) as the other two properties are trivially satisfied.

We follow the same proof as the semi-discrete case in Theorem 2.1. Denoting $c_{h,i}^n := \exp(u_{h,i}^n)$, $\mu_{h,i}^n := u_{h,i}^n + \frac{z_i e}{k_B T} \phi_h^n \in V_h^{k,m,n}$, and taking test function $v_i = \mu_{h,i}^n$ in (9a), we get

$$\int_{I^n} \int_{\Omega} \frac{\partial c_{h,i}^n}{\partial t} \mu_{h,i}^n \, dx dt + \int_{\Omega} \left(c_{h,i}^{n,+} - c_{h,i}^{n-1,-} \right) \mu_{h,i}^{n,+} \, dx + \int_{I^n} \int_{\Omega} D_i c_{h,i}^n |\nabla \mu_{h,i}^n|^2 \, dx dt = 0.$$
 (11a)

A simple calculation yields that

$$\int_{I^n} \int_{\Omega} \frac{\partial c_{h,i}^n}{\partial t} u_{h,i} \, dx dt = \int_{I^n} \frac{d}{dt} \int_{\Omega} U(u_{h,i}) \, dx dt = \int_{\Omega} U(u_{h,i}^{n,-}) \, dx - \int_{\Omega} U(u_{h,i}^{n,+}) \, dx,$$

where $U(\eta) := \exp(\eta)(\eta - 1)$. By Taylor expansion we have

$$(\exp(a) - \exp(b))a = U(a) - U(b) + \frac{1}{2}\exp(\xi)(a-b)^2$$

for some ξ between a and b. Hence,

$$\int_{\Omega} \left(c_{h,i}^{n,+} - c_{h,i}^{n-1,-} \right) u_{h,i}^{n,+} dx = \int_{\Omega} \left(U(u_{h,i}^{n,+}) - U(u_{h,i}^{n-1,-}) + \frac{1}{2} \exp(\xi_{h,i}^{n}) (u_{h,i}^{n-1,-} - u_{h,i}^{n,+})^{2} \right) dx$$

for some $\xi_{h,i}^n$ between $u_{h,i}^{n-1,-}$ and $u_{h,i}^{n,+}$. Combining the above two equalities and summing the terms (11a) over all the indices i, we get

$$\sum_{i=1}^{N} \left(\int_{\Omega} U(u_{h,i}^{n,-}) dx - \int_{\Omega} U(u_{h,i}^{n-1,-}) dx \right) + N_{1,h}^{n} + I_{c,\phi} + \underbrace{\int_{I^{n}} \int_{\Omega} \sum_{i=1}^{N} D_{i} c_{h,i}^{n} |\nabla \mu_{h,i}^{n}|^{2} dx dt}_{-\text{Dise}^{n}} = 0, \tag{11b}$$

where $N_{1,h}^n$ is the following numerical dissipation term from upwinding

$$N_{1,h}^n := \int_{\Omega} \sum_{i=1}^N \frac{1}{2} \exp(\xi_{h,i}^n) (u_{h,i}^{n-1,-} - u_{h,i}^{n,+})^2 dx \ge 0,$$

and the term $I_{c,\phi}$ is given as follows:

$$I_{c,\phi} := \int_{I^n} \int_{\Omega} \frac{\partial S_h^n}{\partial t} \phi_h^n \, \mathrm{d}x \mathrm{d}t + \int_{\Omega} \left(S_h^{n,+} - S_h^{n-1,-} \right) \phi_{h,i}^{n,+} \, \mathrm{d}x,$$

with $S_h^n := \sum_{i=1}^N \frac{z_i e}{k_B T} c_{h,i}^n + \frac{\rho_0}{k_B T}$ being the source term in (9b), where we used the fact that ρ_0, z_i, k_B, T are independent of time. Next, taking $\psi = \partial_t \phi_h^n/(k_B T) \in \mathsf{V}_h^{k,m-1,n}$ in Eq. (9b) and combining with the above term, we get

$$\begin{split} I_{c,\phi} &= -\int_{I^{n}} \int_{\Omega} \frac{\partial}{\partial t} (\frac{\epsilon}{2k_{B}T} |\nabla \phi_{h}^{n}|^{2}) \, \mathrm{d}x \mathrm{d}t + \int_{I^{n}} \int_{\Omega} \frac{\partial}{\partial t} (S_{h}^{n} \phi_{h}^{n}) \, \mathrm{d}x \mathrm{d}t + \int_{\Omega} \left(S_{h}^{n,+} - S_{h}^{n-1,-} \right) \phi_{h,i}^{n,+} \, \mathrm{d}x, \\ &= \int_{\Omega} \left(-\frac{\epsilon}{2k_{B}T} |\nabla \phi_{h}^{n,-}|^{2} + \frac{\epsilon}{2k_{B}T} |\nabla \phi_{h}^{n,+}|^{2} + S_{h}^{n,-} \phi_{h}^{n,-} - S_{h}^{n-1,-} \phi_{h}^{n,+} \right) \, \mathrm{d}x, \\ &= \int_{\Omega} \left(S_{h}^{n,-} \phi_{h}^{n,-} - \frac{\epsilon}{2k_{B}T} |\nabla \phi_{h}^{n,-}|^{2} + \frac{\epsilon}{2k_{B}T} |\nabla (\phi_{h}^{n,+} - \phi^{n-1,-})|^{2} - \frac{\epsilon}{2k_{B}T} |\nabla \phi_{h}^{n-1,-}|^{2} \right) \, \mathrm{d}x \\ &+ \underbrace{\int_{\Omega} \left(\frac{\epsilon}{2k_{B}T} |\nabla \phi_{h}^{n,-1,-} - (S_{h}^{n-1,-}) \phi_{h}^{n,+} \right) \, \mathrm{d}x,}_{=0 \text{ by (9c)}} \\ &= \int_{\Omega} \left(\frac{\epsilon}{2k_{B}T} |\nabla \phi_{h}^{n,-}|^{2} + \frac{\epsilon}{2k_{B}T} |\nabla (\phi_{h}^{n,+} - \phi^{n-1,-})|^{2} - \frac{\epsilon}{2k_{B}T} |\nabla \phi_{h}^{n-1,-}|^{2} \right) \, \mathrm{d}x, \end{split}$$

where the last step is again due to (9c) by taking the test function $\psi = \phi_h^{n,-}/(k_B T)$. Combining the above expression with the equality (11b), we finally get

$$E_h^n + N_{1,h}^n + N_{2,h}^n + \mathsf{Diss}_h^n = E_h^{n-1}$$

where we used the definition of the energy E_h^n and the numerical dissipation term $N_{2,h}^n$ from Theorem 2.2. This completes the proof. \square

Remark 2.3. Our proposed scheme (9) can be also applied to the variable coefficient case to achieve all the three properties in Theorem 2.2. For example, by multiplying all the spatial integrals in 2.2 with a coefficient A(x) > 0, we immediately get a positive and unconditionally energy stable scheme for the following PNP system with a variable (possibly discontinuous) A(x):

$$A\frac{\partial c_i}{\partial t} = \nabla \cdot (AD_i c_i \nabla \mu_i), \quad i = 1, 2, \dots, N,$$
(12a)

$$-\nabla \cdot (A\epsilon \nabla \phi) = A(\rho_0 + \sum_{i=1}^{N} z_i e c_i). \tag{12b}$$

In this case, all the integrals in (10) shall be weighted by the cross-section A(x).

Remark 2.4. While we only proved the energy stability result (10c) for the PNP model with homogeneous Neumann boundary conditions (1d), similar results hold when we replace the Neumann boundary condition for the electrostatic potential ϕ by a Dirichlet or Robin-type boundary condition with minor modifications. For example, if the following homogeneous Robin-type boundary condition for the electrostatic potential is to be used with $\alpha > 0$:

$$\epsilon \frac{\partial \phi}{\partial n} + \alpha \phi = 0, \quad \text{on } \partial \Omega,$$
 (13)

we do not need the compatibility condition $\int_{\Omega} \phi \, dx = 0$ anymore as ϕ is uniquely determined, instead, we need to add a boundary mass term $\int_{\partial\Omega} \alpha \phi_h \psi \, ds$ to Eq. (6b) in the semi-discrete scheme (6), and add the term $\int_{I^n} \int_{\partial\Omega} \alpha \phi_h^n \psi \, ds$ dt to Eq. (9b) and $\int_{\partial\Omega} \alpha \phi_h^{n,-} \psi^{n,-} \, ds$ to (9c) in the fully discrete scheme (9) to reflect the Robintype boundary condition (13). In this case, the energy stability result (10c) would still hold with an additional (non-negative) boundary term $\int_{\partial\Omega} \frac{\alpha}{2k_BT} (\phi_h^{n,-})^2 \, ds$ in the discrete energy (10d), and an additional boundary term $\int_{\partial\Omega} \frac{\alpha}{2k_BT} (\phi_h^{n,+} - \phi_h^{n-1,-})^2 \, ds$ in the numerical dissipation term $N_{2,h}^n$, essentially following the same arguments in the proof of Theorem 2.2.

2.4. Nonlinear system solver and adaptive time stepping

We use Newton's method to solve the fully discrete nonlinear system (9). A sparse direct solver is used for the linear algebraic systems in each Newton's iteration. The Newton's iteration is stopped when the relative error of the energy (10d) is reduced by a factor of 10^{-8} .

One main advantage of unconditionally energy stable schemes with arbitrary order is that they can be easily implemented with an adaptive time stepping strategy so that the time step is dictated only by accuracy rather than by stability as with conditionally stable schemes. Here we use the classical PI step size control algorithm [20]: given a previous time step size Δt^{n-1} , the next time step size Δt^n is proposed as

$$\Delta t_{temp} = \left(\frac{tol}{e_n}\right)^{K_I} \left(\frac{e_{n-1}}{e_n}\right)^{K_P} \Delta t^{n-1}, \qquad \Delta t^n = \min\{\Delta t_{temp}, \theta_{\text{max}} \Delta t^{n-1}, \Delta t_{\text{max}}\}, \tag{14}$$

where tol is a prescribed error tolerance, $\Delta t_{\rm max}$ is a user defined maximum allowed time step size, and

$$e^n := \left| \frac{E_h^n - E_h^{n,lo}}{E_h^n} \right| \tag{15}$$

is the error estimator based on the relative error in energy between the scheme (9) (with temporal order $m \ge 1$) and a companion (temporal) low-order scheme (with m = 0) with the same spatial discretization, and we use the following parameters suggested in [20]:

$$K_P = 0.13$$
, $K_I = 1/15$, $\theta_{\text{max}} = 2$, $\rho = 1.2$.

We reject the proposed Δt^n in (14) if either the Newton iteration did not converge or the target tolerance is violated $(e^n > \rho tol)$. In this case, we halve the time step size by setting $\Delta t^n := 0.5 \Delta t^{n-1}$ and redo the computation.

Remark 2.5. We note that while the convergence of the above Newton's method for the nonlinear system (9) is not theoretically guaranteed, this adaptive time stepping strategy works quite well in practice; see Figs. 5 and 9 for the Newton iteration counts. Specifically in these figures, we observe that the average number of iteration counts is about 3–4, and there are only a few locations (around time t = 240) where the iteration counts are greater than 4.

Assuming sufficiently close initial guess to the true solution and/or sufficiently small time step size, the Newton's method is expected to converge. But quantifying the convergence property of the Newton's algorithm is a highly nontrivial task, which we do not investigate in this work. In this direction, we mention the work [23] which investigated a Newton solver of the backward Euler scheme [9]. In particular, in [23, Theorem 3.2], the authors proved the well-posedness of a linearized PNP system when the domain is convex and the mesh is sufficiently refined. However the convergence of the Newton's algorithm was not theoretically proven therein.

3. Numerics

In this section, we present several numerical examples to validate our theoretical results in the previous section. Our numerical simulations are performed using the open-source finite-element software NGSolve [24], https://ngsolve.org/. In particular, NGSolve's add-on library ngxfem, https://github.com/ngsxfem/ngsxfem, is used in the implementation of the space-time finite element scheme (9). In all the examples, we choose the initial guess for the Newton's algorithm to be the solution at previous time level.

Example 1

(Accuracy test) We first use a manufactured solution example to test the accuracy of the scheme (9). We consider the PNP equations (1) with N=2, $z_1=1$, $z_2=-1$, $e=k_B=T=D_1=D_2=\epsilon=1$. The computational domain is a unit square, and we take source terms such that the smooth exact solution is

$$c_1(t, x, y) = 1 + 0.5 \sin(t) \sin(\pi x) \sin(\pi y),$$

$$c_2(t, x, y) = 1 - 0.5 \sin(t) \sin(\pi x) \sin(\pi y),$$

$$\phi(t, x, y) = \sin(t) \sin(\pi x) \sin(\pi y).$$
(16)

size $\Delta t = 2h$.							
k = m	1/h	L^2 -err in u_h^1	Rate	L^2 -err in u_h^2	Rate	L^2 -err in ϕ_h^2	Rate
1	8	5.228e-03	_	1.362e-02	_	2.140e-02	_
	16	1.473e - 03	1.828	3.821e - 03	1.834	5.461e - 03	1.970
	32	3.923e - 04	1.908	1.000e - 03	1.934	1.374e - 03	1.991
	64	1.016e-04	1.950	2.552e-04	1.970	3.442e - 04	1.997
2	8	1.218e-04	_	2.615e-04	_	1.999e-04	_
	16	1.407e - 05	3.113	1.928e - 05	3.762	1.762e - 05	3.504
	32	1.702e-06	3.048	1.782e - 06	3.435	1.869e - 06	3.237
	64	2.106e-07	3.014	1.992e-07	3.162	2.215e-07	3.077
3	8	9.026e-06	_	1.980e-05	_	1.809e-05	_
	16	4.813e-07	4.229	1.115e-06	4.151	1.083e - 06	4.062
	32	2.768e - 08	4.120	6.665e - 08	4.064	6.651e - 08	4.025
	64	1.675e - 09	4.047	3.990e - 09	4.062	4.122e-09	4.012

Table 1 Example 1. L^2 -errors at time t = 1 for the methods (9) with k = m on a sequence of uniformly refined meshes. Time step size $\Delta t = 2h$

We use homogeneous Dirichlet boundary conditions on u_1, u_2 and ϕ .

We apply the space-time finite element scheme (9) with k = m = 1, k = m = 2, and k = m = 3 on a sequence of uniformly refined triangular meshes. We take uniform time step size $\Delta t = 2h$, where h is the mesh size. The Newton's method converges within 3-4 iterations for all the cases. The L^2 -errors at time t = 1 are recorded in Table 1. Clearly, we observe the expected (k + 1)-th order of convergence for all the variables for the scheme (9) using polynomials of degree k = m.

Example 2

(One-dimensional problem with discontinuous coefficients) Here we solve a two-component (N=2) one-dimensional system (12) with variable discontinuous coefficients. The domain is $\Omega=[-28,25]$, and we use the homogeneous Dirichlet boundary conditions

$$\phi(x) = u_1(x) = u_2(x) = 0 \quad \forall x \in \partial \Omega$$

and initial condition

$$u_1(0, x) = u_2(0, x) = 0.$$

We use the following set of parameters:

$$k_B = T = e = 1, z_1 = 1, z_2 = -1, D_1 = 1, D_2 = 1.0383,$$

$$A = \pi r^2, \text{ with } r(x) = \begin{cases} -0.5x - 7 & \text{if } -28 < x < -18, \\ 2 & \text{if } -18 < x < -5, \\ 0.5 & \text{if } -5 < x < 10, \\ 0.9x - 8.5 & \text{if } 10 < x < 25, \end{cases}$$

$$\epsilon(x) = \begin{cases} 4.7448 & \text{if } -5 < x < -10, \\ 189.79 & \text{elsewhere,} \end{cases}$$

$$\rho_0(x) = \begin{cases} -300 & \text{if } x \in (-2, -1) \cap (0, 1) \cup (2, 3) \cup (4, 5) \cup (6, 7), \\ 0 & \text{elsewhere.} \end{cases}$$

We apply the second-order scheme (9) with polynomial degree k=m=1, and take the initial time stepsize as $\Delta t^1=10^{-4}$. The adaptive time stepping algorithm (14) is used where the companion low order scheme takes k=1 and m=0 on the same mesh. For the two user defined parameters in (14), we take $tol=10^{-3}$, and $\Delta t_{\rm max}=\begin{cases} 2 & \text{if } t<250,\\ 200 & \text{if } t>250. \end{cases}$ The simulation is terminated when relative error in the energy in two consecutive

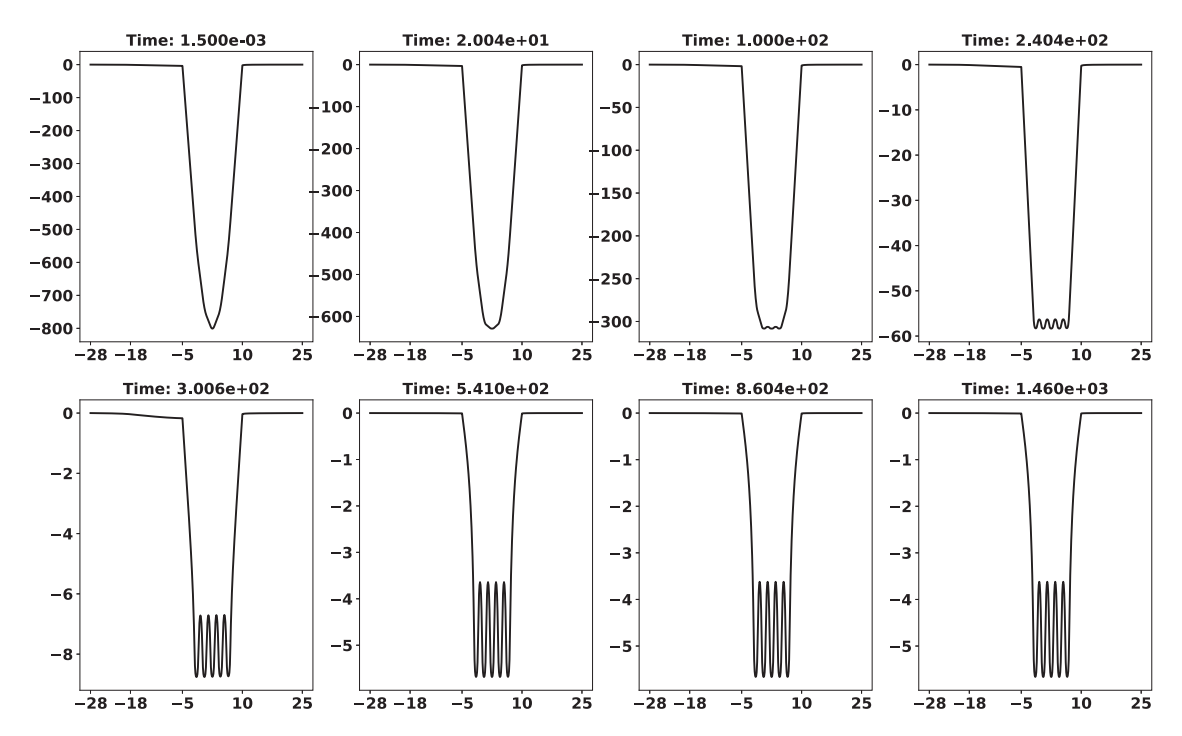


Fig. 1. Example 2. Electrostatic potential ϕ at different times obtained with the scheme (9) with k = m = 1 on a uniform mesh with mesh size h = 1/128.

Table 2 Example 2. Initial and final energy, and total number of time steps to reach the steady state for the scheme (9) with k = m = 1 and adaptive time stepping (14) on different meshes.

Mesh size h	1/16	1/32	1/64	1/128
Initial energy Final energy Total time steps	387788.75	387798.52	387800.97	387801.58
	-3023.3435	-3022.3990	-3022.1619	-3022.1025
	206	208	210	210

time steps is less than 10^{-13} ,

$$\left| \frac{E_h^n - E_h^{n-1}}{E_h^n} \right| < 10^{-13},$$

which indicates a steady state is reached. We find the steady state is reached around time t = 1400.

This problem is very challenging to solve as $c_2 = \exp(u_2)$ stays near zero for $x \in (-5, 10)$ for an extended period of time. Typical solutions at different times are shown in Figs. 1–3, which is obtained by the scheme (9) on a very fine uniform mesh with mesh size h = 1/128. It is clear from Fig. 3 that $c_2 = \exp(u_2)$ stays positive and below $\exp(-50) \approx 2 \times 10^{-22}$ for $x \in (-5, 10)$ and $t \in (20, 240)$, which can be as small as $\exp(-150) \approx 7 \times 10^{-66}$ at around time t = 100. A non positivity preserving scheme may easily lead to a negative density c_2 , hence an early termination of the code using such scheme due to the need to evaluate $\log(c_2)$.

The initial and final energy, along with the total number of time steps to reach the steady state is recorded in Table 2 for four consecutively refined (uniform) meshes. We clearly observe a convergence in the energies as the mesh is refined. Moreover, the total number of time steps to reach the steady state is similar on all four meshes.

We plot in Fig. 4 the energy evolution over time on the four meshes, along with the evolution of the dissipation rates

$$-\frac{E_h^n - E_h^{n-1}}{\Delta t^n}$$
, and Diss_hⁿ/ Δt^n ,

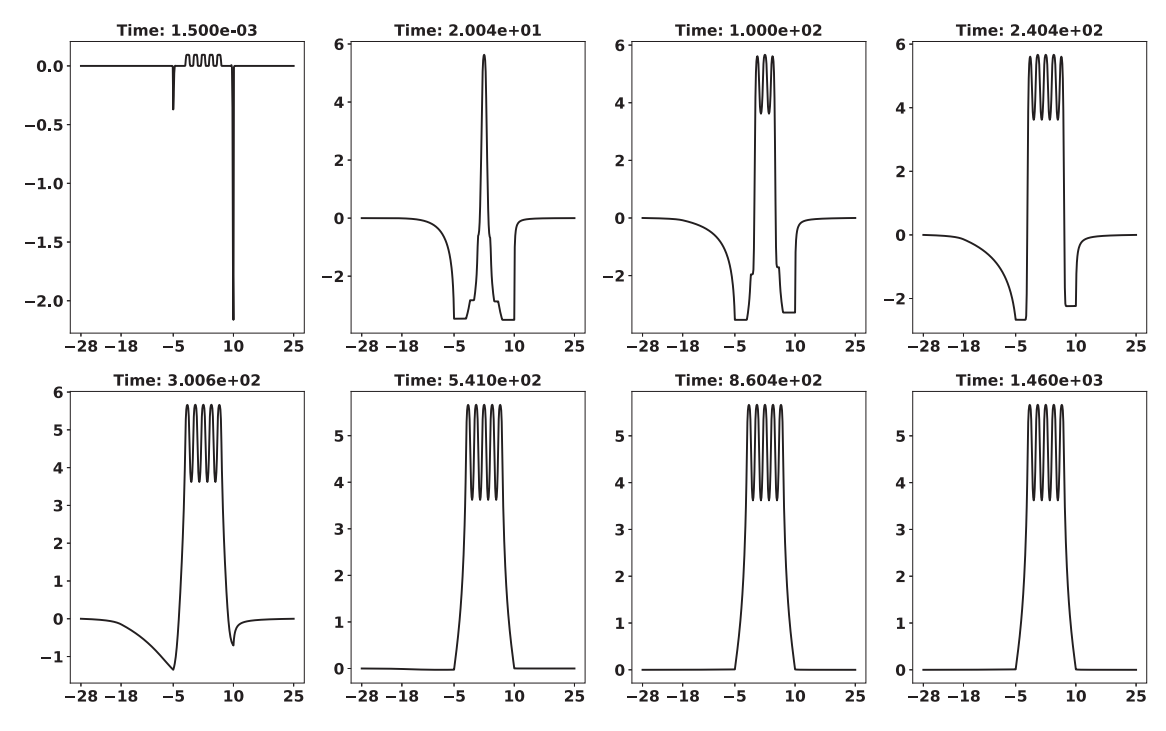


Fig. 2. Example 2. Logarithmic density $u_1 = \log(c_1)$ at different times obtained with the scheme (9) with k = m = 1 on a uniform mesh with mesh size h = 1/128.

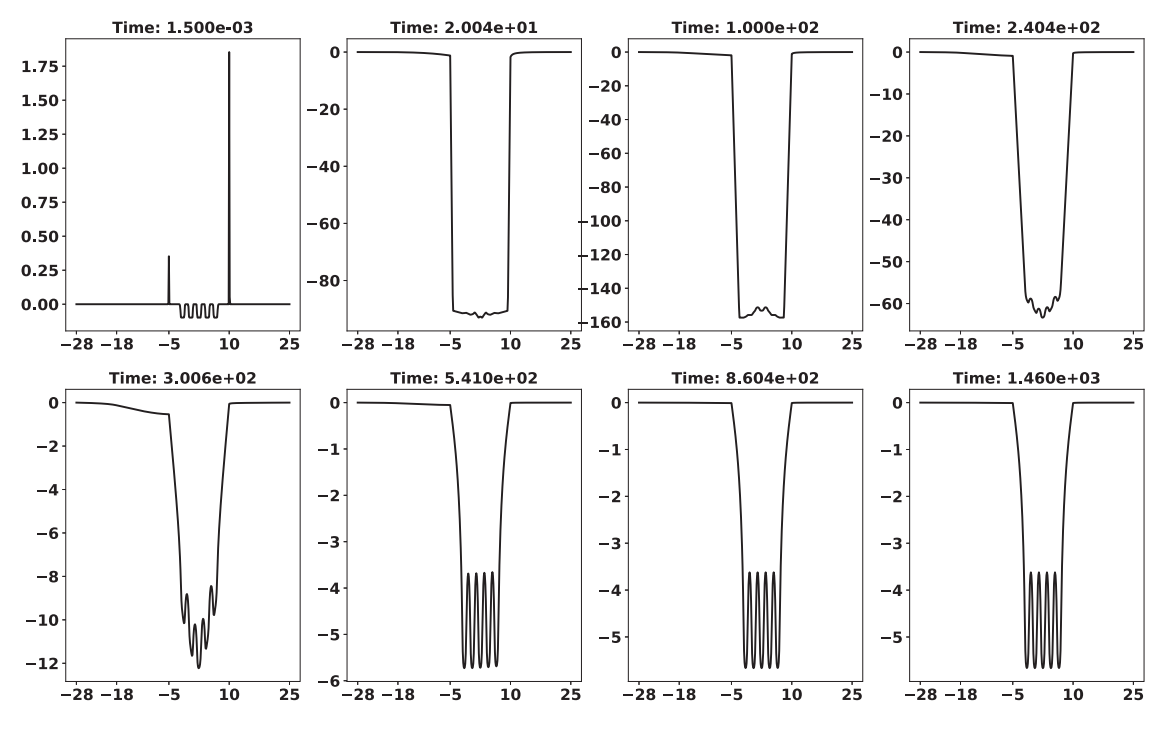


Fig. 3. Example 2. Logarithmic density $u_2 = \log(c_2)$ at different times obtained with the scheme (9) with k = m = 1 on a uniform mesh with mesh size h = 1/128.

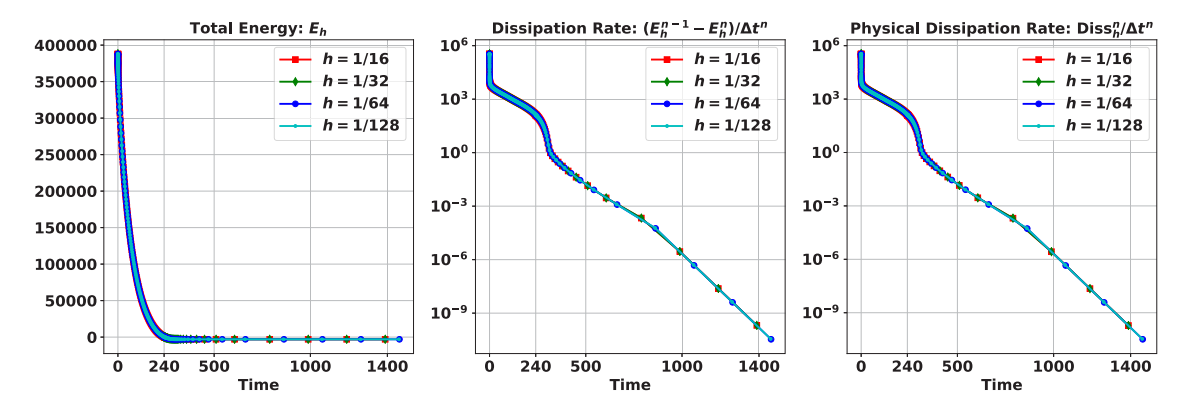


Fig. 4. Example 2. The evolution of energy and dissipation rates over time on the four meshes.

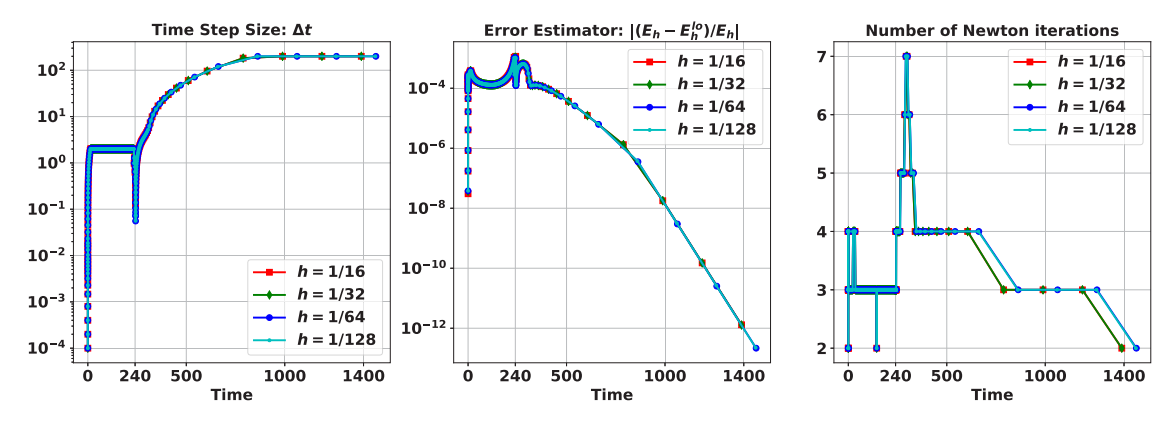


Fig. 5. Example 2. The evolution of time step size Δt^n , error estimator e^n , and Newton iteration number over time on the four meshes.

The results in Fig. 4 numerically confirmed the energy stability result in Theorem 2.2. Moreover, the energy and dissipation rate evolution are very similar on the four meshes, and we also observe that the computed dissipation rate $(E_h^{n-1} - E_h^n)/\Delta t^n$ is very close to and slightly larger than the physical dissipation rate $\mathrm{Diss}_h^n/\Delta t^n$, which is again consistent with the equality (10c) in Theorem 2.2.

Finally we plot in Fig. 5 the evolution of the time step size, the error estimator $e^n = \left| (E_h^n - E_h^{n,lo})/E_h^n \right|$, and the number of Newton iterations. Again, the results on the four meshes are very similar to each other, and the average number of Newton iterations is about 3-4. In particular, we observe that the time step size gradually increases from $\Delta t = 10^{-4}$ to $\Delta t = \Delta t_{\text{max}} = 2$ till time t = 14, then it stays at $\Delta t_{\text{max}} = 2$ for a period of time till around t = 235, where a few drops in time step size occur from t = 235 to t = 243 due to a relative large error e^n . Afterwards, Δt gradually increases to $\Delta t_{\text{max}} = 200$. The advantage of adaptive time stepping is also clearly illustrated in Fig. 5 as a scheme with a uniform time step size $\Delta t = \Delta t^1 = 10^{-4}$ would need about 1.4×10^7 time steps to converge to steady state, while our adaptive time stepping scheme only needs about 200 time steps as shown in Table 2.

Example 3

(Two-dimensional problem with discontinuous coefficients) Here we solve a problem similar to Example 2 on a two-dimensional geometry. The computational domain is shown in Fig. 6. We solve the variable-coefficient PNP equations (12) on the domain Ω using the same set of parameters as in Example 2, with the only exception that the cross-section term is taken to be $A(x) = \pi r(x)$ to take into account the 2D geometry. Homogeneous Dirichlet boundary conditions are imposed on the left and right boundaries segments OA and PF, and homogeneous Neumann boundary conditions are imposed on the rest of the domain boundary.

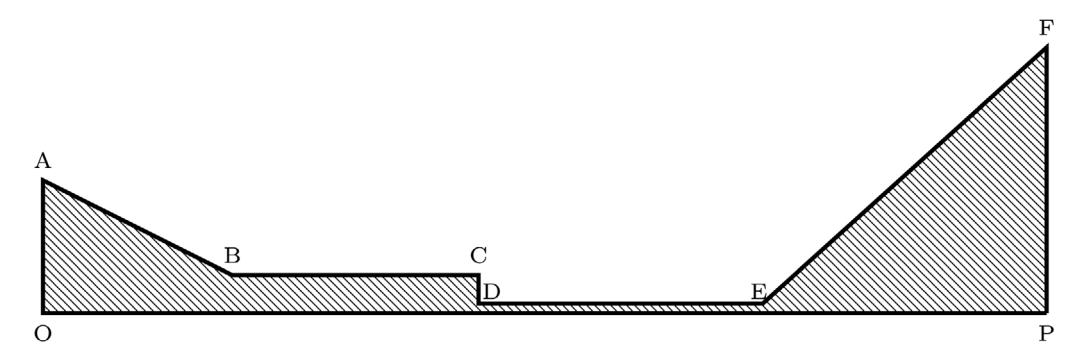


Fig. 6. Example 3. Computational domain Ω (polygon). Coordinates for the vertices: A: (-28, 7), B: (-18, 2), C: (-5, 2), D: (-5, 0.5), E: (10, 0.5), F: (25, 14), O: (-28, 0), P: (25, 0).

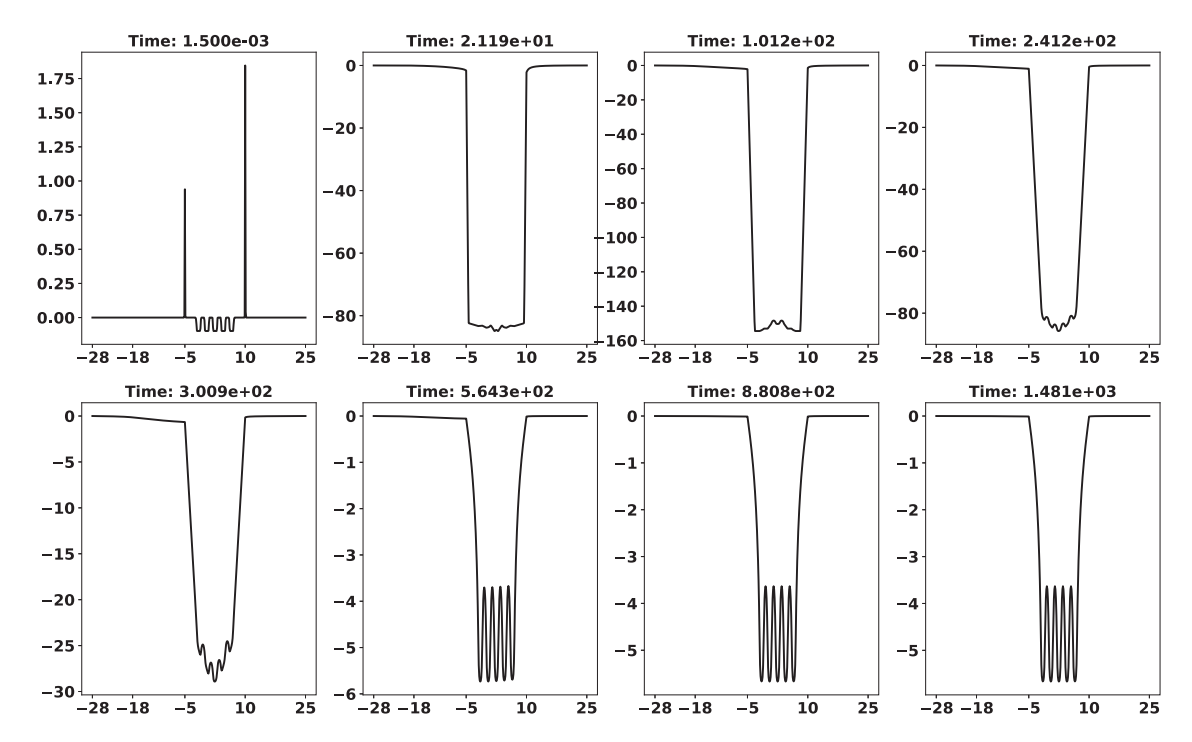


Fig. 7. Example 3. Logarithmic density $u_2 = \log(c_2)$ along cut line y = 0 at different times obtained with the scheme (9) with k = m = 1 on a uniform unstructured mesh with mesh size h = 1/32 (4.43 × 10⁵ triangular elements).

The same second-order scheme (9) with polynomial degree k = m = 1 and adaptive time stepping (14) is used here on three uniform unstructured meshes. The coarse mesh with mesh size h = 1/16 has 1.10×10^5 elements which leads to a total of 3.37×10^5 degrees of freedom (DOFs). The medium mesh with mesh size h = 1/32 has 4.43×10^5 elements which leads to a total of 1.34×10^6 DOFs. The fine mesh with mesh size h = 1/64 has 1.77×10^6 elements which leads to a total of 5.34×10^6 DOFs. We use this example to show the performance of our method in a challenging two-dimensional problem with variable coefficient and complex geometry.

The computational results are very similar to the 1D case in Example 2. Hence, we only present in Fig. 7 the evolution of $u_2 = \log(c_2)$ at different times along the centre cut line y = 0. In particular, we still observe that $c_2 = \exp(u_2)$ stays near zero for $x \in (-5, 10)$ for an extended period of time.

We present in Table 3 the initial and final energy and the total number of time steps to reach the steady state, in Fig. 8 the energy evolution and the evolution of the dissipation rates, and in Fig. 9 the evolution of the time step size, the error estimator and the number of Newton iterations. Again, all the results are very similar to the 1D case in Example 2.

Table 3 Example 3. Initial and final energy, and total number of time steps to reach the steady state for the scheme (9) with k = m = 1 and adaptive time stepping (14) on different meshes.

Mesh size h	1/16	1/32	1/64
Initial energy Final energy	402624.10 -2918.1776	395346.31 -2969.7288	391737.06 -2995.4971
Total time steps	216	213	212

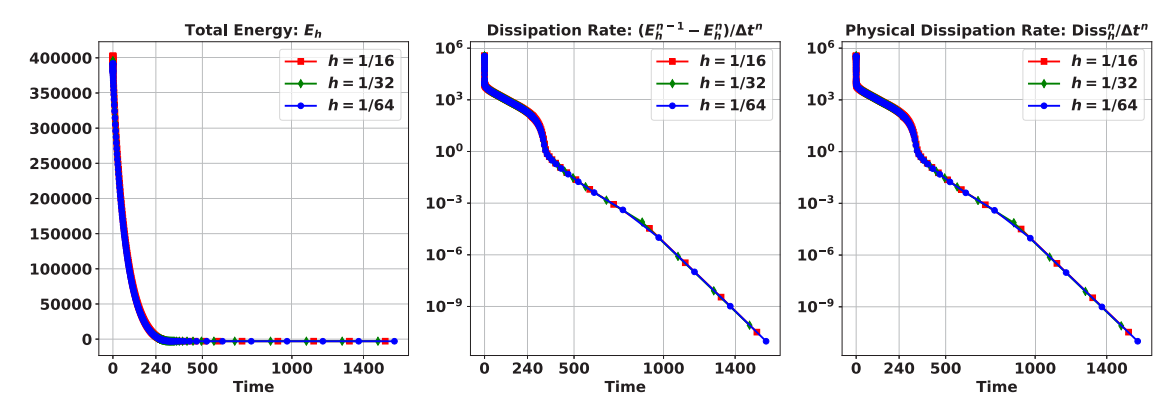


Fig. 8. Example 3. The evolution of energy and dissipation rates over time on the four meshes.

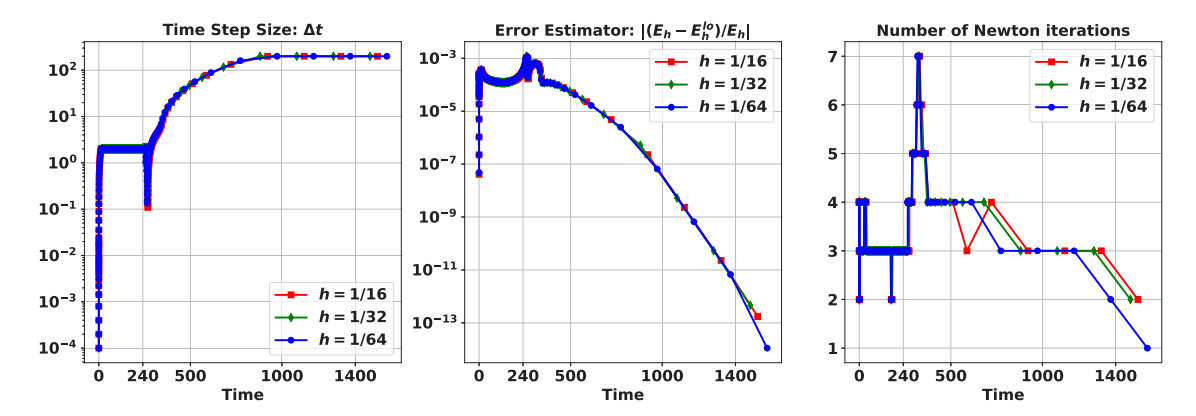


Fig. 9. Example 3. The evolution of time step size Δt^n , error estimator e^n , and Newton iteration number over time on the four meshes.

4. Conclusion

We presented a novel class of high-order accurate, positivity preserving, and unconditionally energy stable space—time finite element schemes for the PNP equations based on discretizing the *entropy variables* associated to the densities. To the best of our knowledge, this is the first class of arbitrarily high-order accurate schemes for PNP equations that is both positivity preserving and unconditionally energy stable.

Our ongoing work consists of extending the STFEM framework to design positivity preserving and unconditionally energy stable schemes for other Wasserstein gradient flow problems, and their coupling with incompressible flows like electrokinetic problems. We are also planning to investigate on alternative finite element discretizations, efficient linear system solvers, and more computationally efficient temporal discretizations for the PNP equations in the future.

Declaration of competing interest

The authors declare that they have no known competing financial interests or personal relationships that could have appeared to influence the work reported in this paper.

Acknowledgement

We would like to thank Christoph Lehrenfeld for suggesting using the space-time framework in the ngsxfem software.

References

- [1] J.W. Jerome, Analysis of Charge Transport: A Mathematical Study of Semiconductor Devices, Springer-Verlag, Berlin, 1996.
- [2] B. Hille, Ion Channels and Excitable Membranes, third Ed., Sinauer Associates, Inc., Sunderland, MA, 2001.
- [3] R.E. Bank, D.J. Rose, W. Fichtner, Numerical methods for semiconductor device simulation, SIAM J. Sci. Stat. Comput. 4 (1983) 416–435.
- [4] A. Prohl, M. Schmuck, Convergent discretizations for the nernst-Planck-Poisson system, Numer. Math. 111 (2009) 591-630.
- [5] B. Lu, M.J. Holst, J.A. McCammon, Y.C. Zhou, Poisson-nernst-Planck equations for simulating biomolecular diffusion-reaction processes I: finite element solutions, J. Comput. Phys. 229 (2010) 6979–6994.
- [6] Q. Zheng, D. Chen, G.-W. Wei, Second-order Poisson-Nernst-Planck solver for ion transport, J. Comput. Phys. 230 (2011) 5239-5262.
- [7] A. Flavell, M. Machen, B. Eisenberg, J. Kabre, C. Liu, X. Li, A conservative finite difference scheme for Poisson-Nernst-Planck equations, J. Comput. Electr. 13 (2014) 235–249.
- [8] D. Meng, B. Zheng, G. Lin, M.L. Sushko, Numerical solution of 3D Poisson-Nernst-Planck equations coupled with classical density functional theory for modeling ion and electron transport in a confined environment, Commun. Comput. Phys. 16 (2014) 1298–1322.
- [9] M.S. Metti, J. Xu, C. Liu, Energetically stable discretizations for charge transport and electrokinetic models, J. Comput. Phys. 306 (2016) 1–18.
- [10] J. Hu, X. Huang, A fully discrete positivity-preserving and energy-dissipative finite difference scheme for Poisson-Nernst-Planck equations, Numer. Math. 145 (2020) 77–115.
- [11] H. Liu, W. Maimaitiyiming, Efficient, positive, and energy stable schemes for multi-D Poisson–Nernst–Planck systems, J. Sci. Comput. 87 (2021) Article number 92.
- [12] J. Shen, X. Jie, Unconditionally positivity preserving and energy dissipative schemes for Poisson–Nernst–Planck equations, Numer. Math. 148 (2021) 671–697.
- [13] C. Liu, C. Wang, S.M. Wise, X. Yue, S. Zhou, A positivity-preserving, energy stable and convergent numerical scheme for the Poisson-Nernst–Planck system, Math. Comp. 90 (2021) 2071–2106.
- [14] F. Huang, J. Shen, Bound/positivity preserving and energy stable SAV schemes for dissipative systems: applications to Keller-Segel and Poisson-Nernst-Planck equations, SIAM J. Sci. Comput. 43 (2021) A1832–A1857.
- [15] J. Shen, J. Xu, J. Yang, A new class of efficient and robust energy stable schemes for gradient flows, SIAM Rev. 61 (2019) 474-506.
- [16] A. Harten, On the symmetric form of systems of conservation laws with entropy, J. Comput. Phys. 49 (1983) 151-164.
- [17] E. Tadmor, Skew-selfadjoint form for systems of conservation laws, J. Math. Anal. Appl. 103 (1984) 428-442.
- [18] T.J.R. Hughes, L.P. Franca, M. Balestra, A new finite element formulation for computational fluid dynamics. v. circumventing the babuška-brezzi condition: a stable petrov-galerkin formulation of the stokes problem accommodating equal-order interpolations, Comput. Methods Appl. Mech. Engrg. 59 (1986) 85–99.
- [19] T.J. Barth, Numerical methods for gas-dynamics systems on unstructured meshes, in: Lecture Notes in Computational Science and Engineering, Vol. 5, Springer, 1999.
- [20] K. Gustafsson, M. Lundh, G. Söderlind, A PI stepsize control for the numerical solution of ordinary differential equations, BIT 28 (1988) 270-287.
- [21] D. Kinderlehrer, L. Monsaingeon, X. Xu, A wasserstein gradient flow approach to Poisson-Nernst-Planck equations, ESAIM Control Optim, Calc. Var. 23 (2017) 137–164.
- [22] R.S. Eisenberg (Ed.), Ion Channels in Biological Membranes; Electrostatic Analysis of a Natural Nanotube, vol. 39, 1998.
- [23] A. Bousquet, X. Hu, M.S. Metti, J. Xu, Newton solvers for drift-diffusion and electrokinetic equations, SIAM J. Sci. Comput. 40 (2018) B982–B1006.
- [24] J. Schöberl, C++11 Implementation of Finite Elements in NGSolve, ASC Report 30/2014, Institute for Analysis and Scientific Computing, Vienna University of Technology, 2014.